Solvothermal Morphology Studies: Alkali and Alkaline Earth Molybdates

by **Alexej Michailovski**, **Frank Krumeich**, and **Greta R. Patzke***

Laboratory of Inorganic Chemistry, ETH Hönggerberg, Wolfgang-Pauli-Strasse 10, CH-8093 Zurich
(Phone: +41-1-632 67 43; fax: +41-1-632 11 49, e-mail: patzke@inorg.chem.ethz.ch)

A convenient and systematic solvothermal pathway towards alkali and alkaline-earth molybdates has been established. The solvothermal treatment of a molybdenum-based precursor material (yellow molybdic acid, $MoO_3 \cdot 2\,H_2O$) with ionic additives (alkali or alkaline-earth halides) provides access to a spectrum of molybdates. Their particle morphology can further be addressed by optimizing the reaction conditions. The resulting products cover a wide scope of sizes and morphologies, ranging from molybdenum oxide fibres with high aspect ratios and nanoscale diameters to millimeter-sized crystals of novel alkali molybdates. Both anionic and cationic additives exhibit certain synthetic profiles that offer the perspective of turning this approach into a 'toolbox' for the tailoring of molybdate-based materials.

1. Introduction. – The outstanding catalytic properties of MoO_3 and their mechanistic foundations [1–3] have been in the focus of research activities over the past decades. Consequently, the crystal growth of this versatile material has been studied as well [4][5]. To fully explore the potential of MoO_3 and related molybdates, it would be highly desirable to downscale these substances to the nano regime so that they are accessible as anisotropic nanotools in large quantities *via* simple preparative routines [6–8]. Recently, the first successful formation of anisotropic MoO_3 by means of solvothermal methods has been reported [9][10]. Solvothermal reactions offer a high degree of preparative flexibility, and this synthetic route is predestined to facilitate the development of a future nanotechnology, because it provides control of particle size and gives access to kinetically stable phases [11–13]. Morphology control of inorganic materials [14] is a further preparative challenge that could be tackled by means of solvothermal methods. A multitude of solvothermal syntheses have been published, but there is still plenty of room for experimental work, and a particular need for systematic investigations. The standard autoclave setup remains a 'black box', and, therefore, most key steps of solvothermal reactions are not fully understood up to now [15]. The direct monitoring of a solvothermal processes can only be performed with rather sophisticated *in situ* techniques.

The standard orthorhombic form of MoO_3 serves as a basis for highly efficient catalysts that are widely applied, *e.g.*, in alcohol or methane oxidation. However, there is another modification of MoO_3 that might even bear superior technical potential: hexagonal MoO_3 (h-MoO_3), which displays a porous (3–3.5 Å) framework structure. Considerable preparative effort has been undertaken since the 1970s to synthesize the hexagonal channel structure of h-MoO_3 in pure form. All those approaches, however, had to overcome a crucial problem: the hexagonal channels are highly dependent on the stabilizing presence of large cations, which are extremely difficult to remove [16–19]. Even the most-successful routes towards pure h-MoO_3 have not afforded the

entirely dehydrated material [20][21]. The cation exchange (alkali *vs.* ammonium ions) and subsequent thermal decomposition of hexagonal molybdates has been established as a route to h-MoO_3 [22]. The preparation of hexagonal molybdates, however, has never been explored beyond standard procedures, with no further parameter variations such as the dissolution of M_2MoO_4 (M = alkali-metal cation) phases in acids, followed by either heating at atmospheric pressure or a few days of solvothermal treatment.

During our systematic investigations, we have already developed highly efficient solvothermal syntheses of $(NH_4)_x(W,Mo)O_3$ nanorods [23] and fibrous MoO_3 [24], starting from yellow molybdic acid, $MoO_3 \cdot 2\,H_2O$. Preliminary results [11] pointed out that the aspect ratio of the MoO_3 fibres can be tuned by standard laboratory acids and ionic additives. The solvothermal reaction of $MoO_3 \cdot 2\,H_2O$ in the presence of ionic additives is in the focus of the present study. In order to keep the systems as concise and straightforward as possible, we have opted for alkali and alkaline-earth halides that are subjected to an optimized solvothermal routine.

2. Experimental. – In a standard experiment, 180 mg of $MoO_3 \cdot 2\,H_2O$ (synthesized according to [25]), 2 ml of distilled H_2O, and 1 mmol of the appropriate alkali or alkaline-earth halide were added to a *Teflon*-lined stainless-steel autoclave with a capacity of 23 ml. The autoclave was then sealed, heated at 180° for 2 d, and subsequently cooled to r.t. The resulting precipitate was collected by filtration, washed with distilled H_2O, EtOH, and Et_2O, and dried in air. X-ray powder-diffraction analyses were conducted on a *STOE STADI-P2* diffractometer in transmission mode (flat sample holders, graphite monochromated CuK_α radiation) equipped with a position-sensitive detector (resolution *ca.* 0.01° in 2θ). Transmission-electron-microscopy (TEM) investigations were performed on a *Philips CM30ST* microscope operated at 300 kV (LaB_6 cathode). The material was deposited on a perforated carbon foil supported on a copper grid. For scanning-electron microscopy (SEM), performed on a *LEO 1530* (FEG) microscope with 1 kV electrons, samples were dispersed in EtOH and subsequently deposited on a silicon wafer. A *CamScan CS-44* electron microscope with an *EDAX-Phoenix* energy-dispersive X-ray spectrometer (*EDXS*) was employed for approximate elemental analyses. Differential-thermal-analysis/thermogravimetry (DTA/TG) measurements were performed on a *NETZSCH STA 409-C* apparatus between 20 and 1200° at a heating rate of 10 K min^{-1}. Laser-ablation-inductively-coupled-mass-spectrometry (LA-ICP-MS) investigations were performed on an *Elan 6100-DRC*-plus-*ICP-MS* apparatus (*Perkin Elmer/Sciex*).

3. The Interaction of $MoO_3 \cdot 2\,H_2O$ and Alkali Halides: Key Observations. – 3.1. *Solvothermal Reaction Pathways.* 3.1.1. *Additive-Free Reactions.* In the course of our previous investigations on the formation of MoO_3 nanorods [24], we have observed that the reaction pathway depends on the solvent. Neutral, unpolar organic solvents such as toluene exert the same effect as a solvent-free environment and give rise to bundles of agglomerated MoO_3 rods. This indicates that the topotactic dehydration of $MoO_3 \cdot 2\,H_2O$ must be triggered by a polar solvent system such as H_2O or diluted acid to produce well-defined, isolated rods.

The solvothermal treatment of $MoO_3 \cdot 2\,H_2O$ in H_2O at 180° afforded highly anisotropic rods: their average diameter was in the range of 90–130 nm, and the rod length varied from 2 to 4 μm (*Fig. 1, a*). At 80°, fibrous α-$MoO_3 \cdot H_2O$ was isolated as an intermediate product of the topotactic reaction. Concerning the reaction timescale, the rods were already present after 3 h of treatment at 180°, and extended reaction times (2 d) induced the formation of tiny holes on the rod surface (*Fig. 1, b*). When enhanced aspect ratios were required (such as diameters of 200–500 nm and lengths up to 50 μm), the reaction temperature had to be raised to 220° (*Fig. 1, c* and *d*).

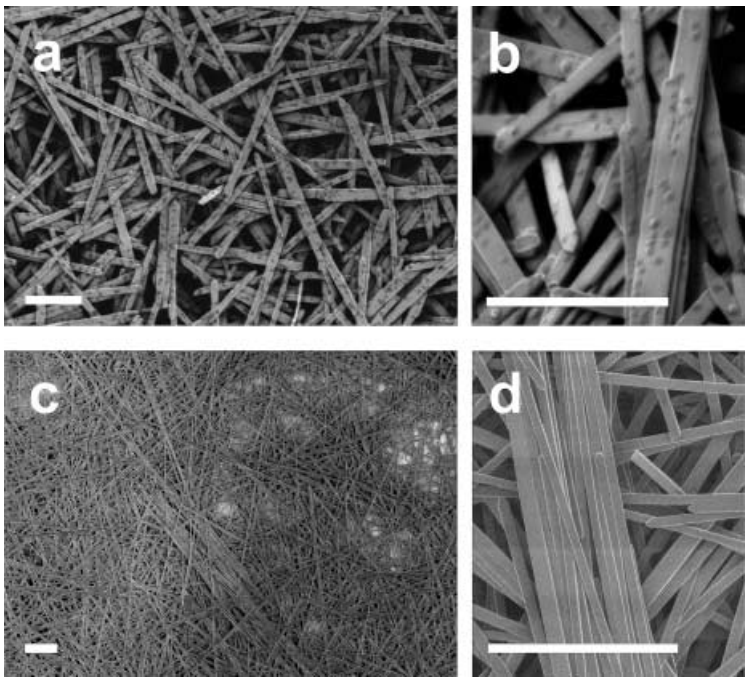

Fig. 1. *Scanning-electron-microscope* (SEM) *images of* MoO_3 *nanorods grown from* $MoO_3 \cdot 2\ H_2O$ *in* H_2O *for 2 days at different temperatures. a*) and *b*) $T = 180°$; scale bar = 1 μm each; the rod surface is becoming porous. *c*) and *d*) $T = 220°$, scale bar = 4 μm; the aspect ratio of the rods is enhanced considerably.

3.1.2. *The Influence of Ionic Additives.* Changing the solvent from H_2O to 25% aqueous AcOH considerably altered the course of the reaction: no intermediates could hitherto be isolated, so that a dissolution/precipitation process appears more reasonable than the topotactic-dehydration route. Further options for tuning the shape and aspect ratio of MoO_3 nanorods are accessible by varying the acidic solvent. In the following, the solvothermal potential of neutral additives was explored. The halide anions were expected to resemble ideal 'spectator' anions with minimum influence on the reaction, which would be predestined for studying the impact of alkali and alkaline-earth cations. This assumption, however, was quickly disproved, because the halide ions turned out to exert a remarkable influence on the course of the solvothermal reaction. Among them, only the chlorides and bromides exhibited analogous behavior (*cf. Tables 1* and *2*), so that they were selected for further investigations. The products emerging from the according $MoO_3 \cdot 2\ H_2O/MX$ ($M = Li^+$ through Cs^+, $X = Cl^-$, Br^-) systems can be subdivided into three main categories (*Table 1*): *1*) LiCl and LiBr afford MoO_3 nanorods; *2*) The reaction of $MoO_3 \cdot 2\ H_2O$ with chlorides and bromides of the heavier alkali cations (Na^+ through Cs^+) leads to the formation of hexagonal molybdates; and *3*) the fluorides/iodides of Rb and Cs give rise to the formation of new alkali-molybdate and -fluoromolybdate modifications (*Table 1*, footnote), as will be discussed in follow-up publications.

Table 1. *Solvothermal-Reaction Products in the System* $MX/MoO_3 \cdot 2\,H_2O$ (M = Li^+ through Cs^+, X = F^- through I^-)

	Li^+	Na^+	K^+	Rb^+	Cs^+
F^-	Dissolution	Dissolution	$K_6Mo_8O_{26}F_2 \cdot 6\,H_2O$	$Rb_6Mo_8O_{26}F_2 \cdot 6\,H_2O$ [a])	$Cs_6Mo_8O_{26}F_2/Cs_2Mo_4O_{13}$ [a])
Cl^-	MoO_3 nanorods	Hexagonal phase	Hexagonal phase (17% K)	Hexagonal phase (13% Rb)	Hexagonal phase (21% Cs)
Br^-	MoO_3 nanorods	Hexagonal phase	Hexagonal phase (16% K)	Hexagonal phase (16% Rb)	Hexagonal phase (21% Cs)
I^-	Amorphous material	Hexagonal phase	$K_2Mo_4O_{13}$ plus hexagonal phase (18% K)	$Rb_2Mo_4O_{13}$ [a]) plus hexagonal phase	$Cs_2Mo_4O_{13}$ [a]) plus hexagonal phase (23% Cs)

[a]) Unknown alkali-molybdate or -fluoromolybdate modification.

3.2. *Adjustment of Solvothermal-Reaction Parameters:* MoO_3 *Nanorods* vs. *Hexagonal Phases.* 3.2.1. *Characterization of* MoO_3 *Nanorods.* The MoO_3 nanorods grown in the presence of LiCl (*Fig. 2*) were slightly shorter than those produced in plain H_2O (diameters ranging from 80 to 120 nm, combined with lengths between 750 nm and 2.2 μm; *Fig. 1, a*, see also *Fig. 11, a*). Their lattice constants ($a = 3.960(1)$, $b = 13.853(3)$, $c = 3.696(1)$ Å) corresponded well with those reported for α-MoO_3 ($a = 3.962$, $b = 13.855$, $c = 3.701$ Å) [26]. The absence of Li^+ in the rods was confirmed by LA-ICP-MS analyses.

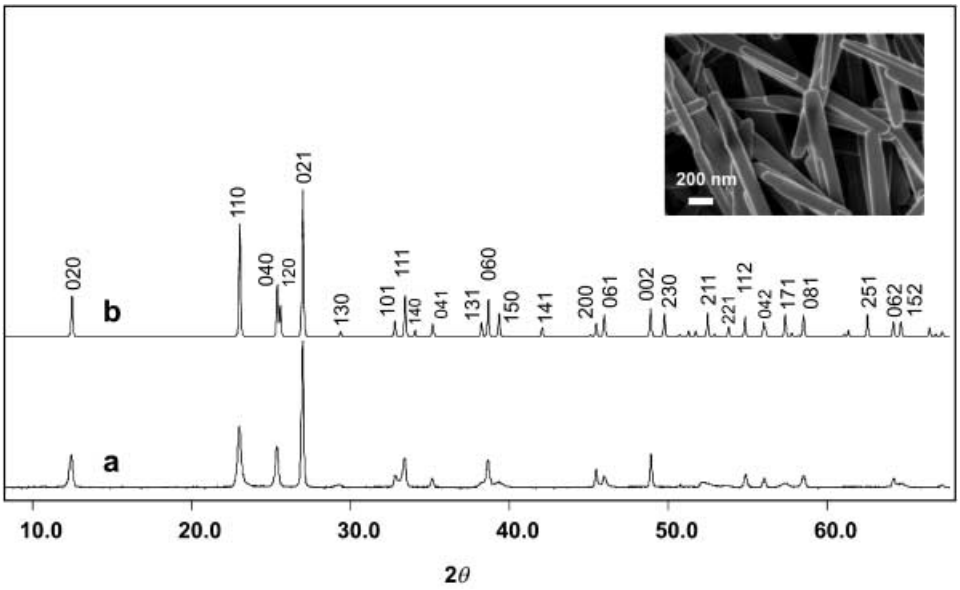

Fig. 2. *X-Ray-diffraction* (XRD) *patterns of* MoO_3 *rods grown in the presence of* a) *LiCl compared to* b) *literature data for* α-MoO_3 [26]. Inset: SEM image of the rods.

3.2.2. *Characterization of Rubidium-Based Hexagonal Molybdates.* A representative characterization of the hexagonal molybdates was performed on a sample of

hexagonal rubidium molybdate grown in the presence of RbBr. The Rb content was *ca.* 16%[1]) (EDX analysis referring to the overall metal content, *cf. Table 1*). This corresponds well to the expected amount of 15.8% based on the empirical formula $RbH_{6x-1}Mo_{6-x}O_{18}$ ($x = 2/3$) [27]. The experimental lattice constants ($a = 10.556(4)$ and $c = 3.734(1)$ Å, *cf. Fig. 3*) were only slightly larger than the literature data ($a = 10.573(1)$, $c = 3.720(2)$ Å) [27]. All columnar hexagonal microcrystals generally displayed diameters ranging from 0.8–4 μm, and lengths from 10 to 40 μm (*Fig. 4*).

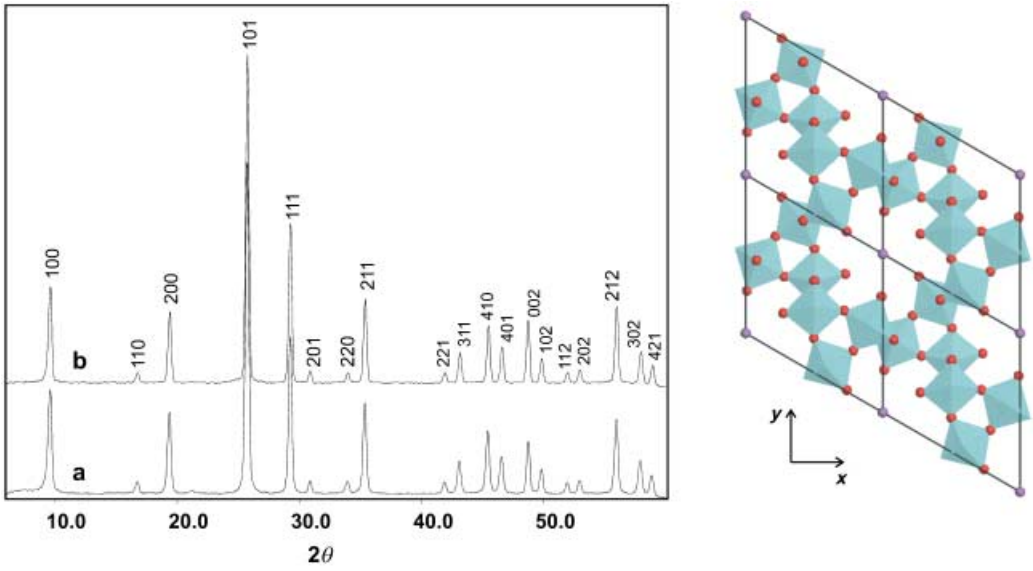

Fig. 3. *XRD Pattern of hexagonal rubidium molybdate* a) *before and* b) *after heating to 400°, together with a representative structural model for hexagonal phases* ($KMo_5O_{15}OH \cdot 2\,H_2O$) [22]

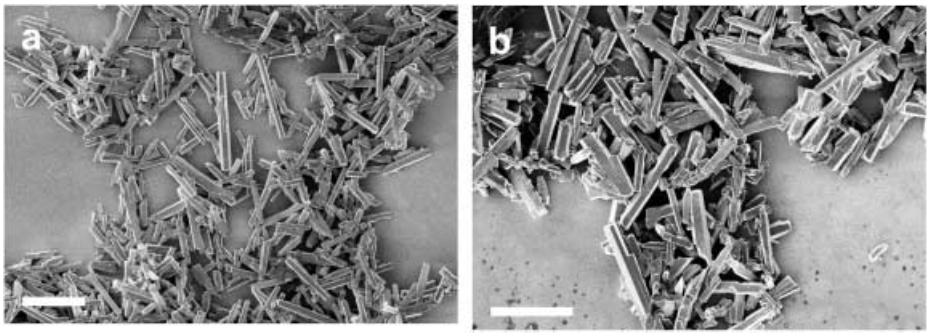

Fig. 4. *SEM Images of hexagonal rubidium molybdate* a) *before and* b) *after heating to 400°* (scale bar = 20 μm)

[1]) Unless specified, elemental compositions are expressed in *atomic* percent.

The thermal behavior of the hexagonal rubidium-molybdate microcrystals was characterized by DTA/TG investigations. Heating to 400° left the columnar shape of the microcrystals intact (*Fig. 4*) and did not affect their XRD pattern (*Fig. 3*). A mass loss of 2.7% was observed. The $RbH_{6x-1}Mo_{6-x}O_{18}$ ($x = 2/3$) model leads to a theoretical mass loss of 3.1%, attributable to H_2O, and the according experimental value has been reported as 3.4% [27]. Concerning the accuracy of the EDX and DTA/TG measurements, the composition of the rubidium-molybdate microcrystals should, thus, be in the range of the literature data [27].

Furthermore, the microcrystals were investigated by means of electron diffraction (*Fig. 5*), which confirmed the hexagonal symmetry. Additional diffuse reflections along the *c**-axis (*Fig. 5,a*) indicated the presence of a fivefold superstructure with a *c*-axis of *ca.* 18.5 Å. This might be due to an ordering of the partially occupied Rb positions inside the channels. HR-TEM Images (*Fig. 6*) showed that the channels were arranged without defects in the *ab*-plane.

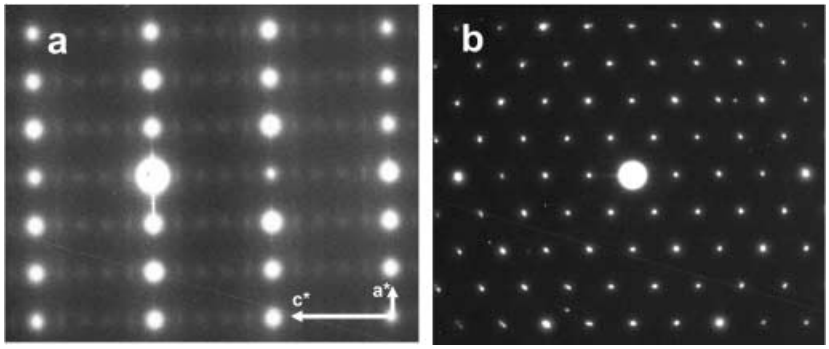

Fig. 5. *Electron-diffraction patterns of hexagonal rubidium molybdate* a) *along [100] and* b) along *[001]*. Parameters: $d_{100} = 9.07$, $d_{001} = 3.70$ Å.

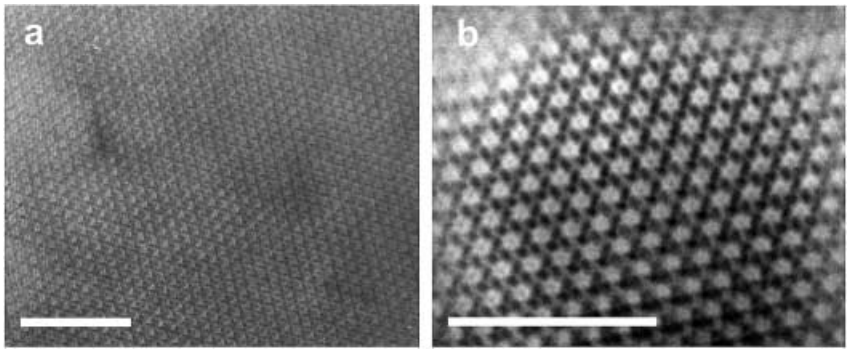

Fig. 6. a) *High-resolution transmission-electron-microscope* (HR-TEM) *image and* b) Fourier-*filtered HR-TEM image of hexagonal rubidium molybdate along [001]* (scale bar = 10 nm). In *b*, the Rb positions are revealed by grey shades that can be seen in the centers of the channels.

3.2.3. *Reaction Pathway.* The formation of MoO_3 nanorods can either proceed *via* topotactic dehydration in H_2O or *via* a dissolution/precipitation sequence in AcOH. In order to garner information about the reaction pathway in the presence of neutral ionic additives, we have employed glass ampoules to monitor the solvothermal reaction of $MoO_3 \cdot 2\,H_2O$ in LiBr (*Fig. 7*) and RbBr solutions, respectively. A reaction period of 48 h was sufficient for quantitative conversion, and in both experiments, a precipitate was present at any stage of the reaction. The only visible phenomena were marginal color changes of the precipitate during the first 90 min. This time interval corresponds well to our previous observations concerning the timescale of rod formation in H_2O: after 3 h of autoclave treatment, the reaction was basically finished [24]. The resulting MoO_3 nanorods formed with LiBr (*Fig. 7*) displayed the same dimensions as their autoclave-grown analogs, and so did the hexagonal rubidium molybdate microcrystals arising from the reaction of $MoO_3 \cdot 2\,H_2O$ and RbBr in a glass ampoule. Both reactions exclusively proceeded in the presence of a solid phase, so that they may be described as 'heterogeneous' solvothermal processes. Accordingly, reactions based on the precipitation from a previously clear solution could then be specified as 'homogeneous' syntheses. As a consequence, *heterogeneous solvothermal reactions do not even require the most elementary pre-treatments such as mixing or dissolution of starting materials, which might render them convenient for technical applications.*

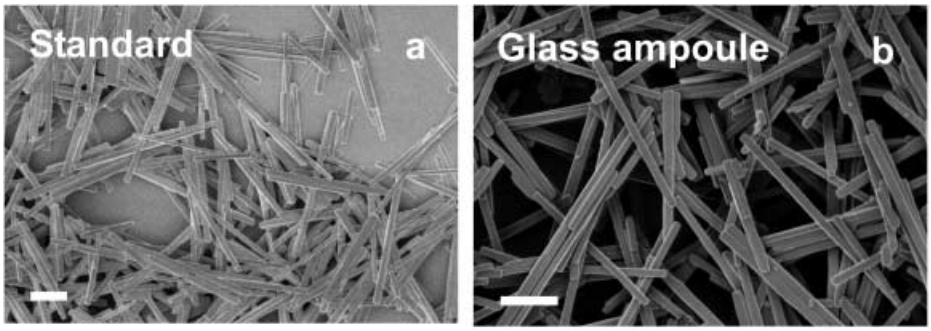

Fig. 7. *SEM Images of MoO_3 nanorods formed in the presence of LiBr as an additive* (scale bar = 1 μm). The products grown in a glass ampoule (*b*) are compared to those grown in a standard autoclave (*a*).

3.2.4. *Concentration of Additives.* Both MoO_3 rods and hexagonal molybdates displayed morphological changes, when the additive concentration was varied. LiBr, for example, was most suitable for MoO_3-rod formation in the 0.5 – 1M concentration range, whereas 2 – 4M solutions gave rise to rod bundles that displayed an increasing degree of agglomeration (*Fig. 8, a* and *b*). Even in the presence of drastically increased Li^+ concentrations, there were no hexagonal molybdates formed at all. The hexagonal rubidium molybdates tended to intergrow as well when the additive concentration was raised: whereas a 1M RbBr solution favored the growth of isolated hexagonal microcrystals (*Fig. 4*), flower-like morphologies (*Fig. 8, c* and *d*) prevailed at higher concentrations (2 – 4M RbBr). The degree of Rb^+ incorporation, however, remained unchanged (13 – 16%, *cf. Table 1*). As a result, *the production of particles with a uniform morphology requires carefully adjusted additive concentrations.*

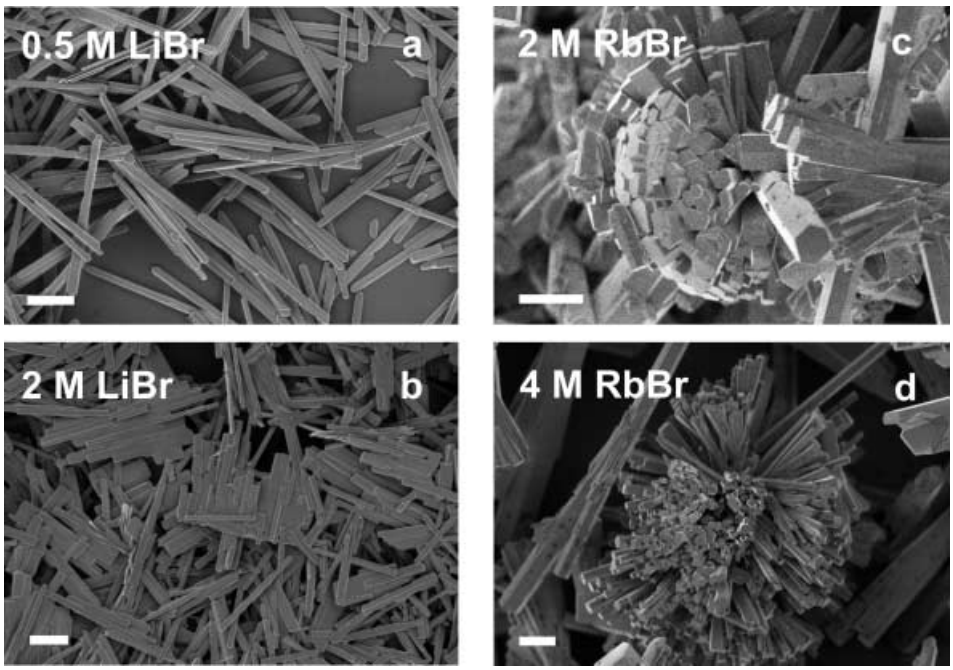

Fig. 8. *SEM Images demonstrating the effect of the concentration of additives on the morphology of* a), b) *MoO_3 nanorods* (0.5 *vs.* 2M LiBr; scale bar = 1 μm) *and* c), d) *hexagonal rubidium molybdate* (2 *vs.* 4M RbBr; scale bar = 6 μm)

3.2.5. *Reaction Temperature.* When MoO_3 nanorods were synthesized in AcOH *via* a homogeneous process, the temperature range of 90–120° gave rise to fine rods with minimum diameters of 40 nm. Their maximum diameter of 150 nm was reached when the temperature was raised to 150° [24]. Rod formation in the presence of an ionic additive, however, required higher reaction temperatures (*ca.* 180°) to prevent rod agglomeration. As shown in *Fig. 9*, treatment of $MoO_3 \cdot 2\,H_2O$ in 1M LiCl solution at 100° partially afforded bundle-like products that finally separated into individual rods

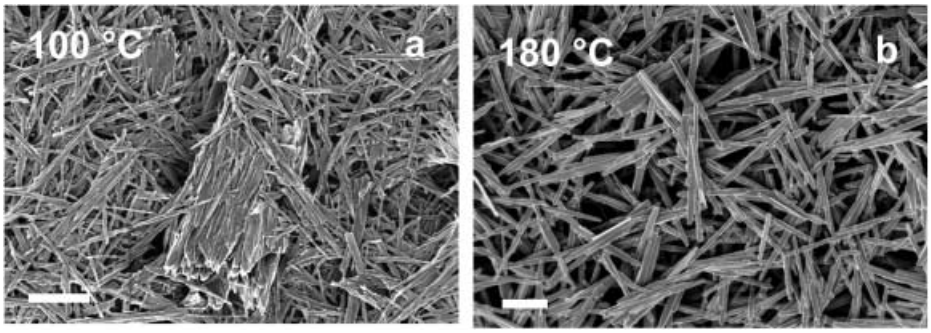

Fig. 9. *SEM Images of MoO_3 nanorods formed in the presence of LiCl at* a) *100° and* b) 180°. Scale bar = 1 μm.

at 180°. Hence, *heterogeneous reactions might require higher temperatures than dissolution/precipitation routes to generate well-separated nanoparticles.*

3.2.6. *Reactions in Acidic Media.* Reference experiments concerning the reaction of $MoO_3 \cdot 2\,H_2O$ with RbCl in acidic media (1%, 5%, and 25% aqueous AcOH) were performed to reveal whether the heavier alkali cations could provide MoO_3 fibres, when subjected to altered reaction conditions. Detailed SEM investigations showed that no MoO_3 nanorods were formed at all. In other words: *the presence of larger alkali cations* (Rb^+, Cs^+) *completely inhibits MoO_3-rod formation.*

3.3. *Sodium-Based Additives: the Interplay of MoO_3 Nanorods and Hexagonal Molybdates.* Depending on the appropriate alkali cation, hydrothermal treatment of $MoO_3 \cdot 2\,H_2O$ either provides MoO_3 nanorods (Li^+) or hexagonal molybdates (K^+ through Cs^+). Na^+ Ions, however, represent a borderline case, leading to mixtures of both phases; the small ionic radius of Na^+ does not suffice to stabilize the hexagonal framework. As a result, sodium is incorporated as $Na^+ \cdot 2\,H_2O$ [27].

3.3.1. *Sodium-Halide* (NaX) *Concentration* (X = Cl, Br). *Fig. 10, a–f* illustrates how the NaX concentration affects the ratio of MoO_3 nanorods to hexagonal sodium molybdate in the reaction products. Lower NaCl concentrations (*ca.* 0.25M) led to the formation of almost phase-pure MoO_3 nanorods, containing *ca.* 5% hexagonal microcrystals as a side product (*Fig. 10, a*). When the concentration was raised to 0.5M NaCl, a mixture containing equal amounts of both phases was obtained. The standard concentration of 1M NaCl yielded hexagonal sodium molybdate as the main product, and the fraction of fibrous MoO_3 side products was just above the XRD detection limit (*Fig. 10, b*). Finally, 2–4M NaCl solutions yielded pure hexagonal sodium molybdate (*Fig. 10, c*). With NaBr as an additive, the above trend was confirmed for concentrations of 0.25M (*Fig. 10, d*) and 1M (*Fig. 10, e*) up to 2M NaBr (pure hexagonal phase). Raising the NaBr concentration to 4M, however, re-introduced MoO_3 fibres into the solvothermal system (*Fig. 10, f*). Hence, *the NaCl or NaBr concentration must be carefully adjusted in the 0.25–2M range to generate phase-pure products.*

3.3.2. *Reaction Temperature.* The influence of the temperature on the reaction of $MoO_3 \cdot 2\,H_2O$ in 1M NaCl solution is summed up in *Fig. 10, g–i*. At 100°, well-shaped and phase-pure microcrystals were obtained (*Fig. 10, g*), with no traces of MoO_3 nanorods being present. Raising the reaction temperature to 140° (*Fig. 10, h*) did not affect the phase purity, but the morphology of the hexagonal phase was beginning to deteriorate. Under standard conditions (180°), MoO_3 nanorods were beginning to emerge (*Fig. 10, b*), and the reaction at 220° finally led to a noticeable amount of coarse MoO_3 microfibers (*Fig. 10, i*). They were smaller and less homogeneous than the fibers generated in an additive-free environment at 220° (*Fig. 1, c–d*).

In summary, *low NaX* (X = Cl, Br) *concentrations and high reaction temperatures favor the formation of MoO_3 nanorods, and the overall solvothermal process is quite sensitive towards parameter shifts. The heavier alkali chlorides and bromides exclusively provide phase-pure products.*

4. The Interaction of $MoO_3 \cdot 2\,H_2O$ with Alkaline-Earth-Based Additives. – 4.1. *General Trends. Table 2* provides a survey of key results concerning the interaction of alkaline-earth additives and $MoO_3 \cdot 2\,H_2O$. They resemble the behavior of the

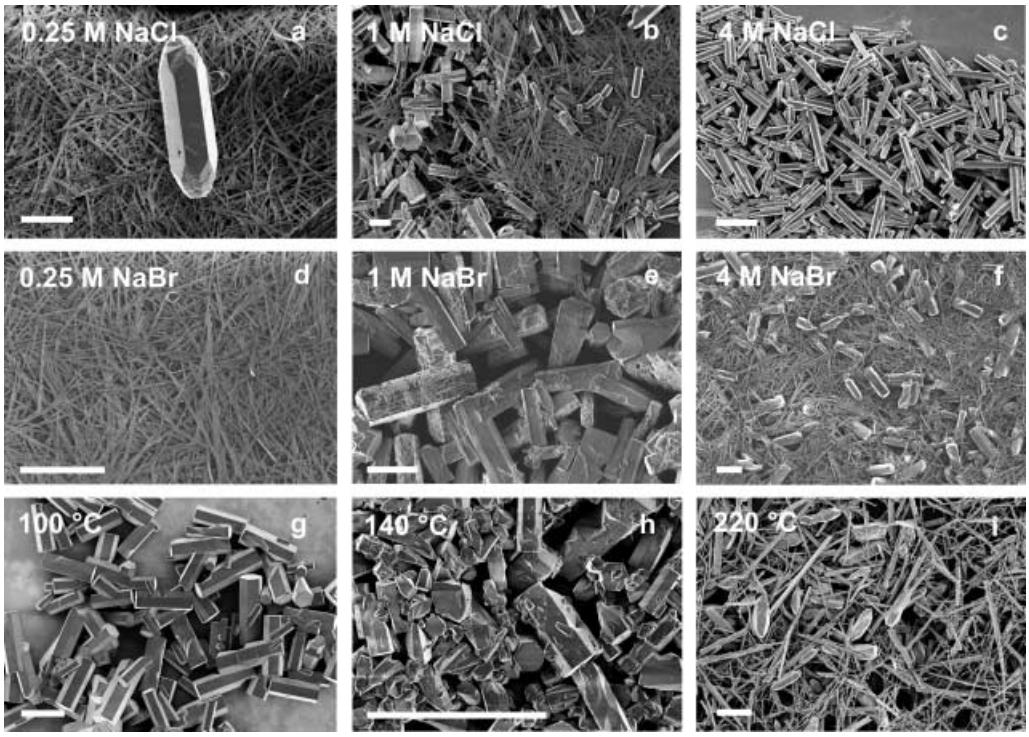

Fig. 10. *SEM Images of MoO_3 nanorods produced in concentration-* (*a–f*) *and temperature-dependent* (*g–i*) *reactions from $MoO_3 \cdot 2\,H_2O$ in the presence of sodium-based additives. a*) 0.25M NaCl, *b*) 1M NaCl, *c*) 4M NaCl, *d*) 0.25M NaBr, *e*) 1M NaBr, *f*) 4M NaBr. The reaction was also performed at constant NaCl concentration (1M) at different temperatures: *g*) 100°, *h*) 140°, and *i*) 220°. The scale bars are 10 μm (*a–c*) or 6 μm (*d–i*), resp.

Table 2. *Solvothermal-Reaction Products of the Alkaline-Earth Hydroxides and Halides with $MoO_3 \cdot 2\,H_2O$ under standard conditions*

	Mg^{2+}	Ca^{2+}	Sr^{2+}	Ba^{2+}
OH^-	Phase unknown	$CaMoO_4$	$SrMoO_4$	$BaMoO_4$
F^-	MoO_3 nanorods plus MgF_2	MoO_3 nanorods plus CaF_2	$SrMo_4O_{13} \cdot 2\,H_2O$	$Ba_2MoO_3F_4$
Cl^-	MoO_3 nanorods	MoO_3 nanorods	$SrMo_4O_{13} \cdot 2\,H_2O$	Hexagonal phase (14% Ba)
Br^-	MoO_3 nanorods	MoO_3 nanorods	$SrMo_4O_{13} \cdot 2\,H_2O$	$Ba_2Mo_4O_{13} \cdot 2\,H_2O$ plus hexagonal phase (13% Ba)
I^-	Amorphous material	Amorphous material	$SrMo_4O_{13} \cdot 2\,H_2O$	$Ba_2Mo_4O_{13} \cdot 2\,H_2O$ plus amorphous material

corresponding alkali-based systems (*Table 1*): *1*) The choice of the counteranion is crucial for the course of the reaction. *2*) Fluorides and iodides trigger the formation of either microcrystalline molybdates or amorphous material. MgF_2 and CaF_2 give rise to MoO_3-rod formation, but due to their low solubility under the reaction conditions, these results were confirmed by additional experiments under more-drastic conditions

(1M HCl, 220°). *3*) The alkaline-earth bromides and chlorides again display analogous solvothermal behavior, and they are the only anions supporting the quantitative formation of MoO_3 nanorods. *4*) The alkaline-earth hydroxides give rise to the formation of $MMoO_4$ phases (M = Ca, Sr, Ba).

4.2. *Trends in the Formation of MoO_3 Nanorods.* MoO_3 Rods are accessible in the presence of the smallest alkali and alkaline-earth cations only: Li^+, Ca^{2+}, and Mg^{2+}.

4.2.1. *Influence of Cations.* The MoO_3 rods obtained with LiCl (*Fig. 11, a*) and $MgCl_2$ (*Fig. 11, d*) exhibited similar dimensions (*ca.* 80-nm diameters and lengths ranging from 600 nm to 2 μm). This might be due to the related electrostatic parameters of Li^+ and Mg^{2+}. The presence of additive ions slightly diminished the aspect ratio with respect to the particles grown in H_2O (*Fig. 1, a* and *b*). This trend was continued with LiBr (*Fig. 11, b*) and $MgBr_2$ (*Fig. 11, e*), and the latter already induced rod agglomeration. Finally, $CaCl_2$ and $CaBr_2$ (*Fig. 11, g* and *h*) quantitatively yielded MoO_3 rod bundles. The various MoO_3-rod dimensions determined are summed up in *Table 3*. Three preparative guidelines can be derived from these results: *1*) The most straightforward additive-based formation of MoO_3 rods proceeds with Li^+ and Mg^{2+} ions. Na^+ Ions represent a borderline case and require optimized reaction conditions. *2*) Compared to the reference reaction in bulk H_2O, Li^+- and Mg^{2+}-based additives slightly downsize the aspect ratio of the rods, whereas Na^+ cations yield considerably longer fibres. *3*) Maximum rod sizes are achieved at elevated temperatures (220°) in pure H_2O.

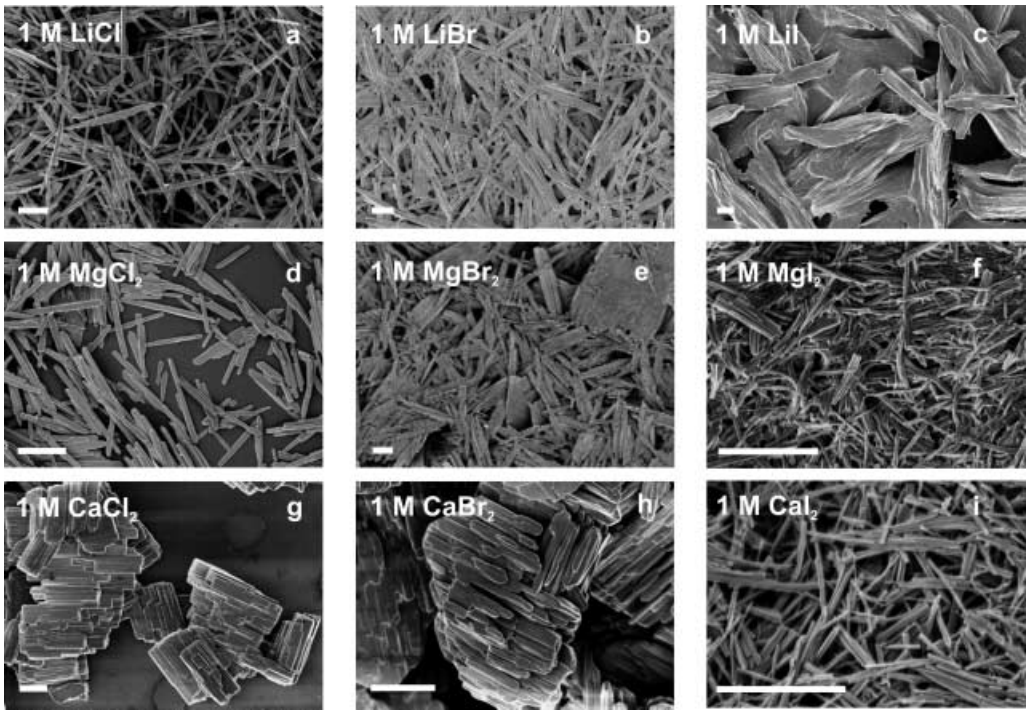

Fig. 11. *SEM Images of rod-shaped solvothermal-reaction products of $MoO_3 \cdot 2\ H_2O$ under standard conditions with* a)–c) *lithium-based,* d)–f) *magnesium-based, and* g)–i) *calcium-based additives.* Scale bars = 1 μm.

Table 3. *Size Trends among MoO_3 Nanorods*

Growth Conditions	Diameter [nm]	Length [μm]
1M LiCl, 180°	80–120	0.75–2.2
1M $MgCl_2$, 180°	80	0.6–2
H_2O, 180°	90–130	1.8–4
0.25M NaCl, 180°[a])	170	5–30[b])
0.25M NaBr, 180°[a])	175–350	12[b])
H_2O, 220°	200–500	≤ 44

[a]) Small amounts of hexagonal sodium molybdate formed as a side product. [b]) Partly also longer rods.

4.2.2. *Influence of Anions.* The iodide series of experiments with LiI, MgI_2, CaI_2 (*Fig. 11, c, f*, and *i*, resp.) revealed a deteriorating effect of the lighter iodides on the overall morphology. The aforementioned trend among the cations, however, appears to be inverted: LiI afforded only unstructured, fibrous material, and MgI_2 yielded intergrown rods. Whereas $CaCl_2$ and $CaBr_2$ favored rod-bundle formation, CaI_2 led to the formation of well-defined fibres with diameters of *ca.* 20 nm and typical lengths of 400 nm.

All three products exhibited hitherto unidentified XRD patterns (*Fig. 12*): the less-defined the morphology of the product, the broader the reflections were. Certain analogies in the XRD patterns might point to the formation of similar products. The redox activity of the iodide ion obviously prevents a clear-cut topotactical reaction and might give rise to a reduction of the Mo^{VI}-based parent structure instead. Consequently,

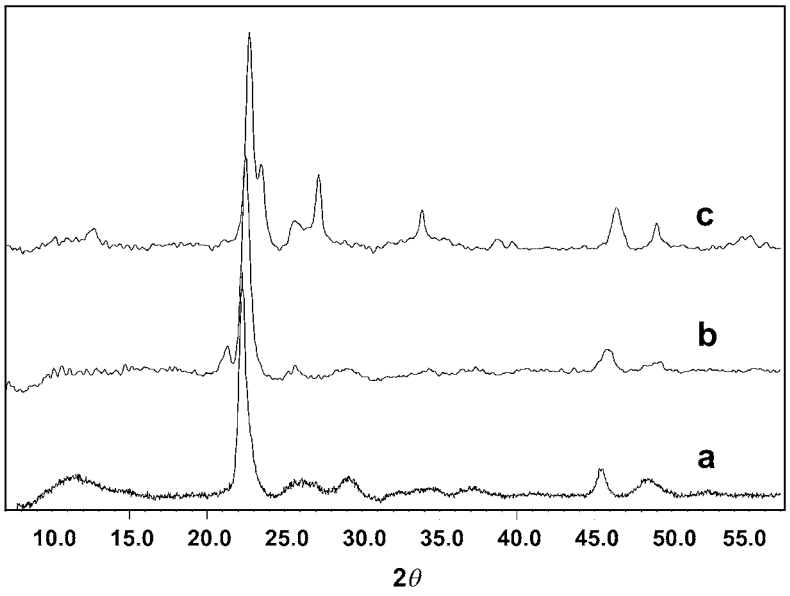

Fig. 12. *XRD Patterns of the fibrous materials grown with* a) *LiI*, b) *MgI_2, and* c) *CaI_2*. See also *Figs. 11, c, f*, and *i*, resp.

neutral and chemically 'inert' counteranions are preferable for morphology studies and nanoparticle production.

4.3. *The Role of Counteranions: Sr- and Ba-Based Additives.* Strontium and barium halides exhibited major differences in their interaction with $MoO_3 \cdot 2\ H_2O$ (*Table 2*). Among them, $BaCl_2$ and $BaBr_2$ exclusively provided alkaline-earth-based hexagonal molybdates.

4.3.1. *Hexagonal Molybdates – an Interesting Class of Channel-Structured Materials.* Only NH_4^+, $Na^+ \cdot 2\ H_2O$, K^+, Rb^+, Cs^+, and $Ag^+ \cdot 2\ H_2O$ have been found to stabilize the channels of hexagonal molybdates [27]. Li^+ Ions have been considered too small to exert a stabilizing effect. To the best of our knowledge, no general and comprehensive study has been performed to investigate the precise criteria required for cation incorporation into hexagonal molybdates. Furthermore, hexagonal molybdates have often been regarded as mere precursor materials for h-MoO_3, although they may well give rise to interesting properties. They provide cation-exchange facilities, and, moreover, structural investigations on molybdate-channel systems are quite challenging, because there are at least two alternative models for rationalizing the charge balance in fully oxidized hexagonal molybdates: electroneutrality might either be achieved in terms of Mo vacancies or by the incorporation of extra O^{2-} ions along with H_2O in the tunnels [20]. The precise interplay of molybdenum vacancies, and of oxo- and hydroxo-groups can only be enlightened with the help of neutron-diffraction methods [20]. Substitution reactions of the molybdenum framework are feasible as well: although Li^+ is too small to stabilize the common hexagonal molybdate structures, it can be incorporated into a vanadium-substituted hexagonal framework resulting in phases of the type $(Li_xH_{1-x})_{0.13}V_{0.13}Mo_{0.87}O_3 \cdot n\ H_2O$ [18]. These substances undergo a 'hopping' transition upon heating that shifts the Li^+ ions on trigonal prismatic sites within the tunnel walls.

4.3.2. *Formation of a Novel Hexagonal Barium Molybdate.* $BaCl_2$ quantitatively yielded a phase-pure hexagonal molybdate containing *ca.* 14% of $Ba^{1)}$. This is a key result, because, to the best of our knowledge, no alkaline-earth-based hexagonal molybdates have been reported up to now. $BaBr_2$ afforded $BaMo_4O_{13} \cdot 2\ H_2O$ as a side product, but the hexagonal barium molybdate could clearly be identified and separated due to its characteristic columnar crystal shape. The aspect ratio of the Ba-containing hexagonal molybdates was considerably smaller with respect to their alkali-based analogs: $BaCl_2$ afforded hexagonal crystals (*Fig. 13, a*) with diameters between 1.5 and 6.5 μm, and lengths ranging from 6 to 20 μm, and $BaBr_2$ (*Fig. 13, b*) further reduced the average crystal dimension to diameters of 1 – 4 μm, and lengths of 4 – 13 μm. The lattice constants for the $BaCl_2$-based product (*Fig. 14*) were determined as $a = 10.514(2)$ and $c = 3.733(1)$ Å.

The newly synthesized hexagonal barium molybdate fits into the established correlation between the ionic radius of an incorporated cation and the resulting volume of the hexagonal unit-cell (*Table 4*) [27]. Ba^{2+} and K^+ display almost the same ionic radii so that their unit-cell volumes are closely related as well. All other alkaline-earth cations failed to yield hexagonal phases under standard reaction conditions: whereas Ba^{2+} (149 pm) is sufficiently large to stabilize the hexagonal framework, Sr^{2+} (132 pm) is obviously too small, and so $SrMo_4O_{13} \cdot 2\ H_2O$ was formed instead. This points to a critical threshold ionic radius of 132 – 150 pm for the formation of hexagonal phases.

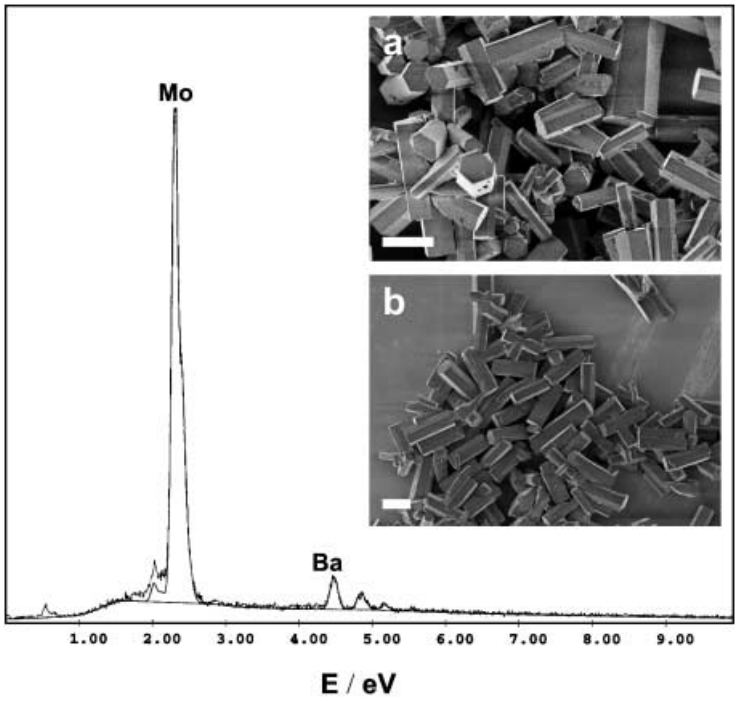

Fig. 13. *SEM Images of hexagonal barium molybdate crystals grown in the presence of* a) *$BaCl_2$ and* b) *$BaBr_2$, together with the EDX spectrum of the latter* (scale bar = 6 μm)

Table 4. *Ionic Radii and Unit-Cell Volumes of Known Alkali-Based Hexagonal Phases Compared to the Newly Synthesized Barium-Containing Phase*

Cation	Unit-cell volume [Å^3]	Ionic radius [pm][a])
Ba^{2+} (new)	357.37(13)	149
K^+ [27]	356.97(17)	152
Rb^+ [27]	360.14(18)	166
Cs^+ [27]	362.35(6)	181

[a]) According to [28], for a sixfold coordination sphere.

To investigate whether Sr^{2+} could still be incorporated into the hexagonal phases *via* a combined solvothermal reaction, a series of experiments, starting from mixtures of $SrCl_2$ and $BaCl_2$ (Sr/Ba ratios of 1:4, 2:3, 3:2, and 4:1), were carried out. Surprisingly, the formation of hexagonal phases broke down altogether, and all main products adopted the MMo_4O_{13} structure.

4.3.3. *Strontium- vs. Barium-Based Additives.* Whereas Ba-based additives afforded a variety of products, their Sr-based counterparts showed a distinct preference for $SrMo_4O_{13} \cdot 2\,H_2O$ (*Table 2*), which might point to an outstanding thermodynamic stability of this phase. Even SrI_2 generated well-developed crystals of $SrMo_4O_{13} \cdot 2\,H_2O$ (*Fig. 15, a*), whereas all other alkali and alkaline-earth iodides mainly gave rise to

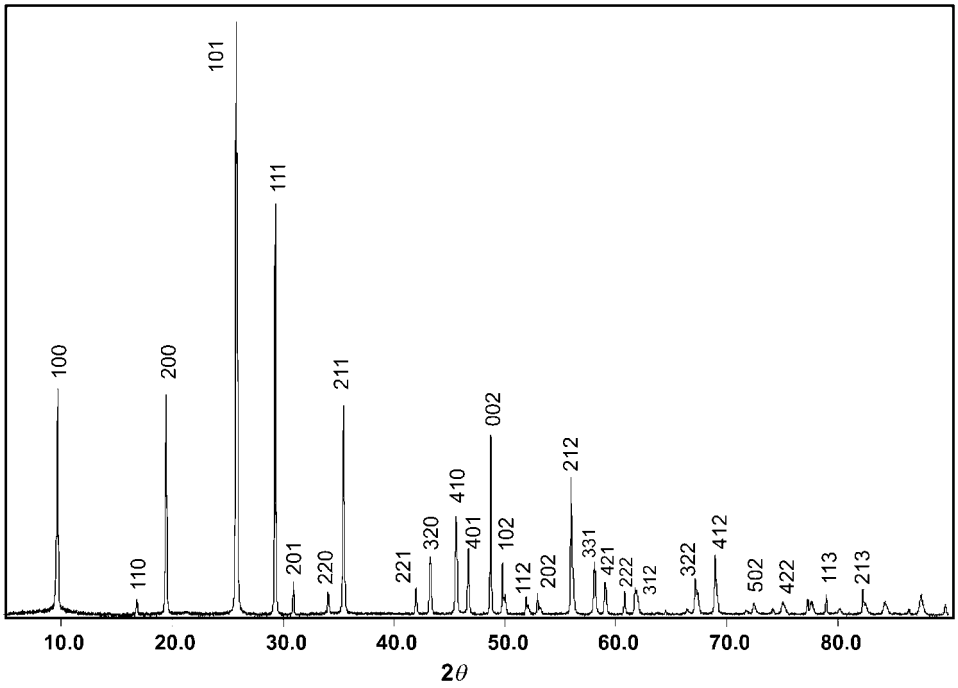

Fig. 14. *XRD Pattern of hexagonal barium molybdate grown from* $MoO_3 \cdot 2\ H_2O$ *in the presence of* $BaCl_2$

amorphous materials. The size of the $SrMo_4O_{13} \cdot 2\ H_2O$ platelets could be adjusted by choosing between $SrBr_2$ and SrI_2: the latter afforded crystals with edges ranging from 25 to 100 μm, and sides between 500 nm and 1 μm (*Fig. 15, a*). $SrBr_2$ downsized the platelet dimensions (*Fig. 15, b*): the smallest crystals were thin squares (200 × 200 nm), and the maximum edge lengths reached 20 μm (max. thickness: 200 nm). Up to the 1990s, the Sr/Mo/O/H system was far from explored, and $SrMoO_4$ and $SrMoO_3$ had been the only well-characterized phases until $SrMo_4O_{13} \cdot 2\ H_2O$ was found to be

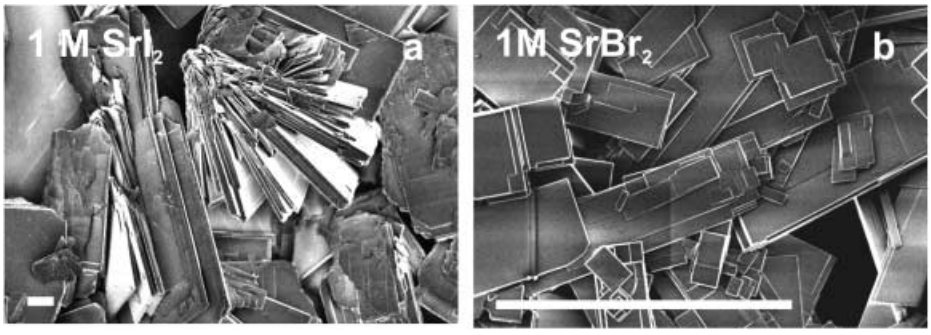

Fig. 15. *SEM Images of platelets of* $SrMo_4O_{13} \cdot 2\ H_2O$ *grown in the presence of* a) SrI_2 *and* b) $SrBr_2$. Scale bar = 10 μm.

isostructural with $BaMo_4O_{13} \cdot 2\,H_2O$ [29]. Infinite sheets of distorted MoO_6 and MoO_5 moieties, sharing edges and vertices, represent the main structural element of the $MMo_4O_{13} \cdot 2\,H_2O$ (M = Sr, Ba) compounds [30]. The original hydrothermal synthesis of single crystals of $SrMo_4O_{13} \cdot 2\,H_2O$ starts from a mixture of SeO_2, $SrCO_3$, and MoO_3. Hence, our new bromide/iodide route represents a selenium-free alternative.

The existence of strontium fluoromolybdates has not been reported hitherto. $Ba_2MoO_3F_4$, however, is a well-known fluoromolybdate that has attracted interest due to its nonlinear optical properties [31]. Furthermore, it has been in the focus of NMR studies concerning the O/F ordering in the chains of corner-sharing MoO/F octahedra separated by Ba cations [32]. The synthesis of $Ba_2MoO_3F_4$ single crystals requires harsh conditions (BaF_2, MoO_3, 3 months of heating at 680°) [33], and even a newly developed hydrothermal approach still requires HF and rather high temperatures (BaF_2/MoO_3, 15 ml of 3.2% aqueous HF solution, 3 d, 227°) [32].

The solvothermal route presented here provides phase-pure microcrystals of $Ba_2MoO_3F_4$ *via* a novel and fairly mild approach. Flower-like aggregates of intergrown microcolumns exhibiting lengths from 1.6 to 6 μm and diameters of *ca.* 0.85 μm (*Fig. 16*) are formed. The constants of the monoclinic lattice were determined as $a = 11.497(8)$, $b = 9.352(6)$, $c = 7.258(6)$ Å, and $\beta = 126.23(7)°$, and they agree well with the literature data ($a = 11.457$, $b = 9.365$, $c = 7.237$ Å, $\beta = 126.30°$) [34].

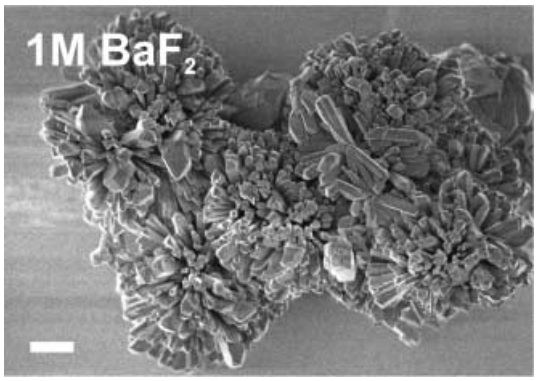

Fig. 16. *SEM Image of flower-like intergrown microcrystals of $Ba_2MoO_3F_4$.* Scale bar = 2 μm.

5. Discussion. – The solvothermal behavior of $MoO_3 \cdot 2\,H_2O$ in the presence of alkali- and alkaline-earth-based halides is summed up graphically in *Fig. 17* and can be discussed with respect to the following criteria.

1) The resulting products can be classified according to the *role of the cation: a*) MoO_3 nanorods are preferably formed with the smallest cations (Li^+, Na^+, Mg^{2+}), and their aspect ratios can be changed accordingly with respect to the reference route in pure H_2O; *b*) The heavier and larger alkali (K^+ through Cs^+) and alkaline-earth cations (Ba^{2+}) are capable of stabilizing the hexagonal molybdate channel structure; *c*) Sr^{2+} Ions exhibit a remarkable tendency towards the formation of the tetramolybdate phase, $SrMo_4O_{13} \cdot 2\,H_2O$, while all remaining additive cations fail to provide phase-pure tetramolybdates.

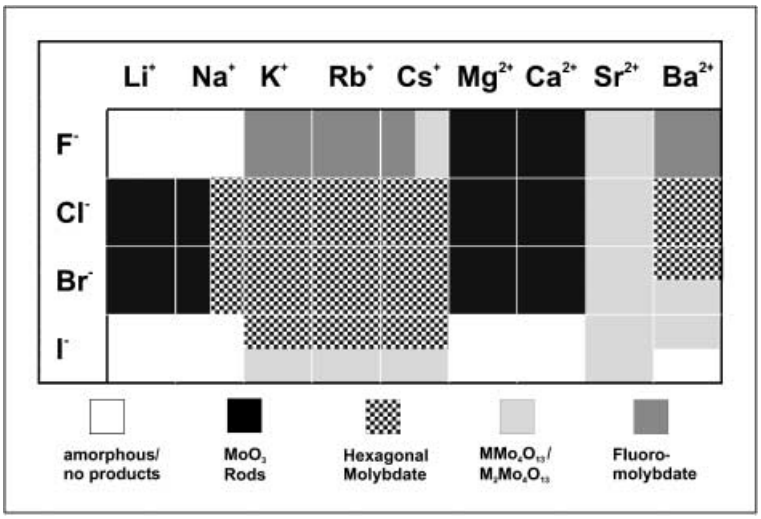

Fig. 17. *Solvothermal-reaction products of* $MoO_3 \cdot 2\ H_2O$ *with alkali and alkaline-earth halides*

2) The *anionic part* of an additive exerts a distinct influence upon the products: *a*) *Fluorides* tend to be incorporated into the products, thus providing a chemically mild access to barium fluoromolybdate, and convenient routes to novel rubidium and caesium molybdate and fluoromolybdate modifications. *b*) *Chlorides and bromides* display an almost entirely identical behavior, and their interference with the solvothermal reaction system is kept to a minimum, which renders them suitable for competitive experiments and morphology studies. *c*) *Iodides* often exert a destructive influence on both phase and morphology of the reaction products due to their redox activity; only tetramolybdates and hexagonal molybdates withstand this tendency.

3) The *product morphologies* cover a wide size range: *a*) The smallest MoO_3 rods exhibit nanoscale diameters, and the larger ones provide enhanced aspect ratios (up to 1:200). *b*) Hexagonal molybdates usually form well-shaped microcrystals. *c*) Especially the novel tetra- and fluoromolybdate modifications tend to form large crystals on the millimeter scale.

In summary, the synthetic strategy employed here provides reasonable access to a wide spectrum of products *via* a simple and straightforward solvothermal routine.

The underlying mechanisms remain to be enlightened: the ionic radii of the additives only provide a useful preparative guideline for addressing certain molybdates, and considerable effort is necessary to fully understand the solvothermal process. Lab-scale quenching experiments provide basic insights, but sophisticated *in situ* techniques are the method of choice. We are currently working on EXAFS experiments *in situ* concerning the formation of MoO_3 nanorods from $MoO_3 \cdot 2\ H_2O$. The interaction of molybdenum-based oxidic precursor materials with alkali iodides and fluorides has been investigated in another systematic study that continues this work and will be presented in a follow-up publication.

6. Conclusions. – Four main trends finally emerge from the present study. *1*) A spectrum of molybdates can be selectively addressed by the appropriate choice of an alkali or alkaline-earth halide. Further morphology tuning is feasible in terms of parameter optimization. *2*) Pathways to novel phases, such as the first Ba-containing hexagonal molybdates, have been established. *3*) The preparative potential of ionic additives is currently explored with respect to other anions/cations and expanded upon quaternary systems. Especially the newly formed Rb and Cs molybdates provide a rich crystal chemistry that serves as a basis for manifold structural studies, including the formation of solid solutions. *4*) The precursor-additive approach may finally be turned into a tailored additive 'toolbox' for the straightforward synthesis and morphology adjustment of molybdates.

All in all, this study might be regarded as a contribution to the challenging task of introducing a 'design' approach into solid-state chemistry.

The authors thank Prof. *R. Nesper* (Laboratory of Inorganic Chemistry, ETH Zurich) for his steady interest and continuous support of this work. Our research was funded by the ETH Zurich, by the *Swiss National Science Foundation* ('*MaNEP – Materials with Novel Electronic Properties*'), and by the *National Research Program* ('*Supramolecular Functional Materials*'). The authors thank *Kathrin Hametner* (group of Prof. *D. Günther*, ETH Zurich) for LA-ICP-MS analyses, and *Christian Mensing* for DTA/TG measurements.

REFERENCES

[1] A. Baiker, D. Gasser, *Z. Phys. Chem.* **1986**, *149*, 119.
[2] H.-F. Liu, R.-S. Liu, K. Y. Liew, R. E. Johnson, J. H. Lunsford, *J. Am. Chem. Soc.* **1984**, *106*, 4117.
[3] A. Baiker, P. Dollenmeier, A. Reller, *J. Catal.* **1987**, *103*, 394.
[4] J. L. Callahan, R. H. Petrucci, C. A. Brown, *Science* **1958**, *128*, 841.
[5] J. Li, P. Wei, W. Ruigang, J. Chen, *Key Eng. Mat.* **2002**, *224–226*, 367.
[6] C. N. R. Rao, A. K. Cheetham, *J. Mater. Chem.* **2001**, *11*, 2887.
[7] C. N. R. Rao, B. C. Satishkumar, A. Govindaraj, M. Nath, *ChemPhysChem* **2001**, *2*, 79.
[8] R. Tenne, *Prog. Inorg. Chem.* **2001**, *50*, 269.
[9] X. W. Lou, H. C. Zeng, *Chem. Mater.* **2002**, *14*, 4781.
[10] M. Niederberger, F. Krumeich, H.-J. Muhr, M. Müller, R. Nesper, *J. Mater. Chem.* **2001**, *11*, 1941.
[11] G. R. Patzke, F. Krumeich, R. Nesper, *Angew. Chem., Int. Ed.* **2002**, *41*, 2446.
[12] R. I. Walton, *Chem. Soc. Rev.* **2002**, *31*, 230.
[13] K. Byrappa, M. Yoshimura, 'Handbook of Hydrothermal Technology', Noyes, Park Ridge, NJ, 2001.
[14] S. Mann, *Angew. Chem., Int. Ed.* **2000**, *39*, 3392; G. A. Ozin, H. Yang, N. Coombs, *Nature (London)* **1997**, *386*, 692; G. R. Patzke, *Angew. Chem., Int. Ed.* **2003**, *42*, 972.
[15] R. I. Walton, F. Millange, R. I. Smith, T. C. Hansen, D. O'Hare, *J. Am. Chem. Soc.* **2001**, *123*, 12547.
[16] N. Sotani, *Bull. Chem. Soc. Jpn.* **1975**, *48*, 1820.
[17] T. P. Feist, P. K. Davies, *Chem. Mater.* **1991**, *3*, 1011.
[18] Y. Hu, P. K. Davies, T. P. Feist, *Solid State Ionics* **1992**, *53–56*, 539.
[19] O. Mougin, J.-L. Dubois, F. Mathieu, A. Rousset, *J. Solid State Chem.* **2000**, *152*, 353.
[20] J. Guo, P. Zavalij, M. S. Whittingham, *J. Solid State Chem.* **1995**, *117*, 323.
[21] Y. Muraoka, J.-C. Grenier, S. Petit, M. Pouchard, *Solid State Sci.* **1999**, *1*, 133.
[22] B. Krebs, I. Paulat-Böschen, *Acta Crystallogr., Sect. B* **1976**, *32*, 1697.
[23] A. Michailovski, F. Krumeich, G. R. Patzke, *Chem. Mater.* **2004**, *16*, 1433.
[24] G. R. Patzke, A. Michailovski, F. Krumeich, R. Nesper, J.-D. Grunwaldt, A. Baiker, *Chem. Mater.* **2004**, *16*, 1126.
[25] J. J. Cruywagen, J. B. B. Heyns, *S. Afr. J. Chem.* **1981**, *34*, 118.
[26] G. Andersson, A. Magneli, *Acta Chem. Scand.* **1950**, *4*, 793.
[27] E. M. McCarron III, D. M. Thomas, J. C. Calabrese, *Inorg. Chem.* **1987**, *26*, 370.
[28] R. D. Shannon, *Acta Crystallogr., Sect A* **1976**, *32*, 751.
[29] W. T. A. Harrison, L. L. Dussack, A. J. Jacobson, *J. Solid State Chem.* **1995**, *116*, 95.

[30] W. T. A. Harrison, *Acta Crystallogr., Sect C* **1999**, *55*, 485.
[31] M. Wiegel, G. Blasse, *Solid State Commun.* **1993**, *86*, 239.
[32] L.-S. Du, F. Wang, C. P. Grey, *J. Solid State Chem.* **1998**, *140*, 285.
[33] G. Wingefeld, R. Hoppe, *Z. Anorg. Allg. Chem.* **1984**, *518*, 149.
[34] R. Domesl, R. Hoppe, *Z. Anorg. Allg. Chem.* **1982**, *492*, 63.

Received November 26, 2003